HNPS Advances in Nuclear Physics

Vol 9 (1998)

HNPS1998

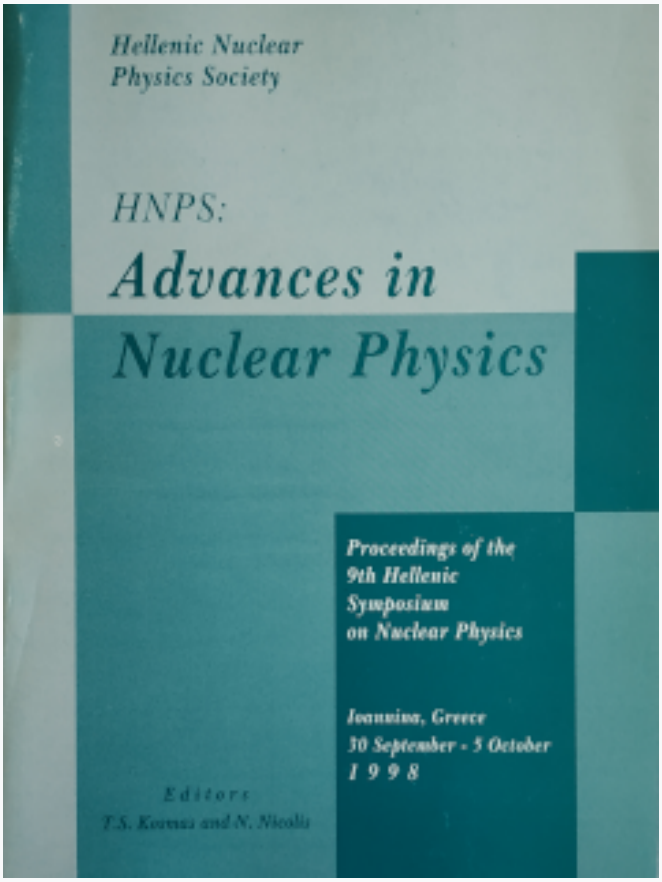

Improved tests of muon and electron flavor symmetry in muon processes

W. R. Molzon

doi: 10.12681/hnps.2777

Improved tests of muon and electron flavor symmetry in muon processes

William R. Molzon

Department of Physics and Astronomy, University of California, Irvine, CA 92697-4575

Abstract

I review the motivation for and status of searches for violation of muon and electron number conservation, concentrating on muon initiated processes. I then discuss the progress expected in the next few years, concentrating on a new experiment, E940 at BNL (the MECO experiment). It will improve the experimental sensitivity for the process $\mu^- N \to e^- N$ to below 10^{-16}, roughly 4 orders of magnitude better than the current limit.

1 Introduction

Since the discovery of the muon, there has been intense experimental and theoretical effort to understand why more than one *family* of leptons exists and how the families are related. The fact that the decay of a muon to an electron and a photon was not observed at the expected level led to the hypothesis that each family of leptons carries an additive quantum number and that these additive quantum numbers are at least approximately conserved. The experimental evidence for conservation of these quantum numbers implies the existence of fundamental symmetries of nature, the source of which is not understood. Within the Standard Model, the conservation could be considered accidental; there is no explicit gauge symmetry for which lepton number is the conserved quantity, but, in the absence of neutrino mass, there is no mechanism for breaking this symmetry. Understanding the family structure of quarks and leptons remains one of the central issues in gaining a better understanding of the fundamental particles and their interactions.

Recently, oscillations between types of neutrinos have been observed by the Super Kamiokande experiment [1,2]. The data is interpreted as implying oscillations between ν_μ and either ν_τ or ν_s, a previously unknown and non-interacting (sterile) neutrinos. This is the first compelling evidence for neutrino mass and

oscillations and the first evidence for violation of electron lepton number. Other evidence also exists for oscillations between ν_μ and ν_e from the LSND collaboration [3] and from the deficit of electron neutrinos from the sun. Since neutrinos have mass and mix, LFV processes involving charged leptons could be induced at the one-loop level. A one-loop diagram for $\mu^- \to e^-\gamma$ is shown in Fig. 1. In the quark sector, flavor changing neutral currents have, of course, been studied for many years; they are understood as arising from quark mixing as described by the quark mixing (CKM) matrix; an example of the kind of diagram contributing to one such decay is also shown in Fig. 1. By extending the Standard Model to include neutrino masses (either Dirac or Majorana), the experimental evidence for neutrino oscillations is readily accommodated.

The observed values of (or limits on) neutrino masses and mixing does not lead to experimentally accessible levels of LFV processes in the charged sector due to the small differences in neutrino masses. Hence, an observation of LFV in the charged lepton sector would be unambiguous evidence for physical processes other than those embodied in the Standard Model, even extended to include massive neutrinos.

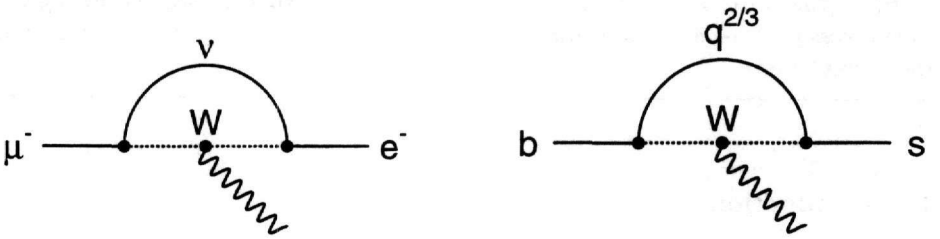

Fig. 1. Feynman diagrams for the process $\mu^+ \to e^+\gamma$ and $b \to s\gamma$ involving a loop containing a W boson and either a charge 2/3 quark or a neutrino

Because there is no Standard Model background to LFV processes, searches for them are among the most sensitive ways to look for physics beyond the Standard Model. There has been recent progress in LFV searches using both kaon and muon processes. We list in Table 1 the LFV processes that have been studied, the current experimental limits on these processes, and their classification in terms of a change in *generation number* in the model of Cahn and Harari [4]. This model presumes that the process occurs at tree level or in a one loop diagram, and infers a mass (or mass difference) limit based on the assumption that the coupling strength is that of the electroweak force. Limits on LFV processes involving the τ lepton ($\tau \to \mu\gamma$) and B meson decays ($B \to \mu e$) have also been set; the sensitivity is limited by both statistics and backgrounds. In both cases, the limits on new physics are typically not nearly as restrictive as those set by experiments using muons and kaons.

The discovery of LFV processes would indicate the existence of either a new force mediated by a new gauge boson with non-diagonal lepton couplings or a

Table 1
LFV violating process, the change in generation number in the model of Cahn and Harari [4], the current experimental limits, and the inferred limits on intermediate particle masses (updated from the reference for new experimental results)

Process	Reference	ΔG	limit	mass limit (TeV)
$K_L^0 \to \mu e$	[5]	0,2	4.7×10^{-12}	150
$K_L^0 \to \pi\mu e$	[6]	0,2	3.2×10^{-10}	37
$K^+ \to \pi\mu e$	[7]	0	2.1×10^{-10}	21
$\mu^+ \to e^+e^+e^-$	[8]	1	1.0×10^{-12}	86
$\mu^+ \to e^+\gamma$	[9]	1	1.2×10^{-11}	21
$\mu^-N \to e^-N$	[10]	1	6.1×10^{-13}	365

new class of heavy particles with lepton flavor mixing in this new sector (e.g. supersymmetry). The possibility of LFV exists in essentially all extensions to the Standard Model, and we will discuss some of these below.

In the remainder of this paper, we will briefly discuss physics models that allow lepton flavor violation and the range in parameter space in these models that can be probed by proposed experiments. We will then give an overview of the experimental techniques involved in $\mu \to e^+\gamma$ and $\mu^-N \to e^-N$ experiments, and discuss the experiments that have given the most stringent limits. Finally, we will describe a new experiment that is proposed to improve very substantially the experimental search for $\mu^-N \to e^-N$.

2 Theoretical Motivation for LFV Searches

Aside from the underlying motivation to test conservation laws with the best possible sensitivity, there is theoretical motivation derived from the many proposed extensions to the Standard Model that allow LFV. In general, these models have not been devised for the purpose of predicting LFV. In many cases, the existing stringent LFV limits already restrict the allowed values of parameters within these models. Feynman diagrams for new processes that could contribute to LFV are shown in Fig. 2. Among the possibilities are a) four fermion contact interactions that couple quarks and leptons, b) leptoquarks with non-diagonal couplings, c) new Z' gauge bosons that couple non-diagonally to leptons, d) non-diagonal couplings of Higgs bosons, e) heavy neutrinos that mix with the known neutrinos, f) supersymmetry models in which LFV occurs in the supersymmetric sector, horizontal gauge bosons that explicitly couple one lepton family to another, etc [11]. In most models, there is no particular scale at which lepton flavor violation should occur,

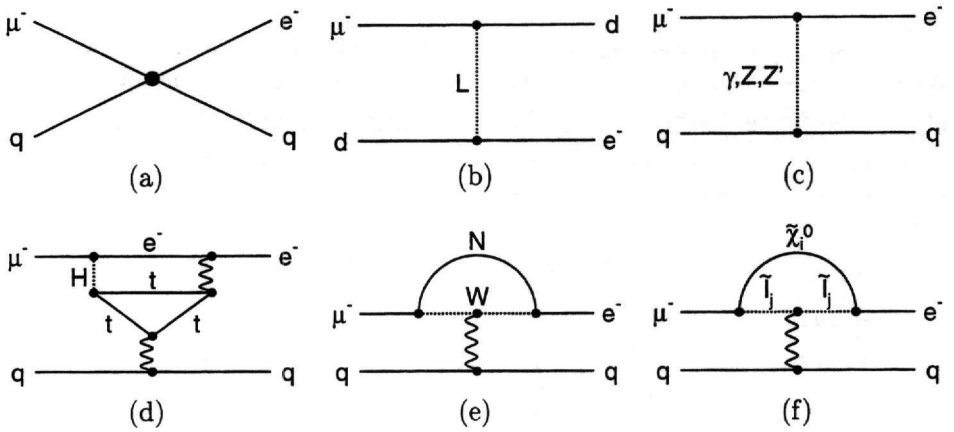

Fig. 2. Feynman diagrams for the process $\mu^- N \to e^- N$ in different scenarios for non Standard Model physics

since masses, coupling strengths and mixing angles of new particles are not predicted. Nonetheless, the reach in parameter space of current and proposed experiments is impressive. For example, in the case of technicolor, the expectation was that lepton flavor violation would occur at levels that are already ruled out, and these models are severely restricted by limits on LFV processes. Similarly, limits on $\mu^- N \to e^- N$ already require $B(Z^0 \to \mu e) < 10^{-13}$, well below what can be measured by direct detection of that decay.

Much interest has occurred recently in supersymmetric models, in particular in grand unified supersymmetric models. It was realized, first by Hall and Barbieri, that LFV will occur at experimentally accessible levels in a large class of supersymmetric models [13–15,12]. Further, in some specific grand unified supersymmetric models, the rate for LFV processes can be related directly to standard model parameters. The predicted rates for the processes $\mu^- N \to e^- N$ and $\mu^+ \to e^+ \gamma$ are shown in Fig. 3 in one such model [12].

If grand unified supersymmetric models actually are realized, a search for $\mu^- N \to e^- N$ with sensitivity 10^{-16} or $\mu^+ \to e^+ \gamma$ with sensitivity 10^{-14} have a real potential for discovering lepton flavor violation. Even if supersymmetry is discovered by direct observation of new particles, the measurement of LFV violating processes will be extremely important in understanding symmetry breaking in the interactions. And perhaps even more importantly, the very large improvements in experimental sensitivity provide a very large discovery potential in many models of new physics.

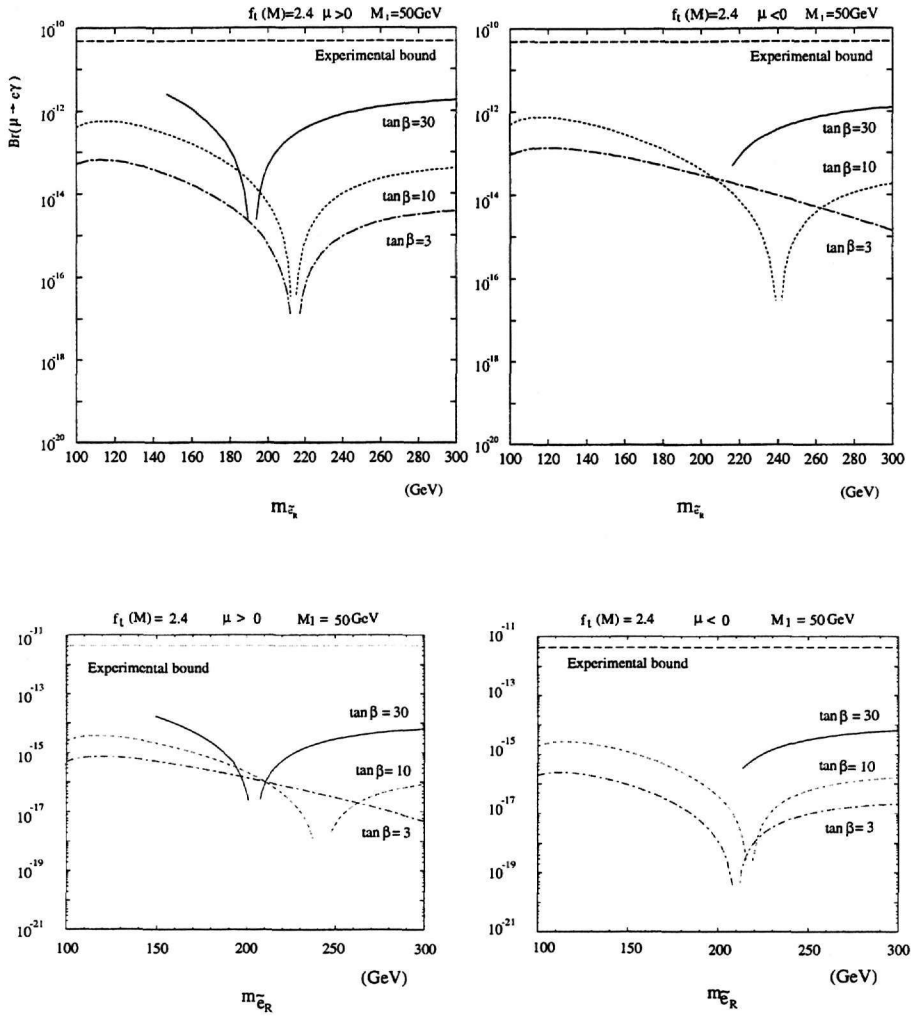

Fig. 3. Expected rates for $\mu^+ \to e^+\gamma$ (*top*) and $\mu^- N \to e^- N$ (*bottom*) in the model of Hisano, *et al.* [12], for different values of the ratio of Higgs particle vacuum expectation values, as a function of the right handed selectron mass. The plots are shown for the parameter $\mu > 0$ (*left*) and $\mu < 0$ (*right*). The bounds on branching ratios for $\mu^- N \to e^- N$ and $e\mu^+ \to e^+\gamma$ have improved to 1.2×10^{-11} and 6.1×10^{-13}, respectively, since this publication

3 Overview of LFV Searches Using Muons

Of the muon initiated LFV processes, the most familiar is $\mu^+ \to e^+\gamma$ decay. This process has been studied extensively, and the sensitivity of searches continues to improve. The best limits on the process are set by the MEGA experiment [9] and there have been discussions about the possibility of doing experiments with even better sensitivity. A second process is $\mu \to eee$; it is

closely related to $\mu^+ \to e^+\gamma$ if mediated by a γ. If so, at the same branching fraction it is less sensitive to the underlying physics due to an extra factor of α in the decay rate. The limit is already very good [8], and there are no proposals to do another experiment. A third reaction is $\mu^- N \to e^- N$; it is also closely related to $\mu^+ \to e^+\gamma$ if mediated by a photon. In this case, for the same underlying physics, the ratio $R_{\mu e} \equiv \Gamma(\mu^- N \to e^- N)/\Gamma(\mu^- N \to \nu N')$ is about 300 times smaller [16] than the branching fraction for $\mu^+ \to e^+\gamma$. There is an ongoing experiment [10] to improve the sensitivity, and a new experiment [17] has been approved to improve it even further.

3.1 $\mu^+ \to e^+\gamma$ Experiments

Searches for $\mu^+ \to e^+\gamma$ are conceptually very simple. The signature is a photon and an electron, each with energy $\sim m_\mu/2$, originating from a common point at the same time, and with opposite momenta.

The experiment is performed by bringing a large flux of μ^+ to rest in a thin target and measuring the kinematic properties of the e^+ and γ from the decay. The principal experimental difficulty lies in suppressing backgrounds. One intrinsic source is radiative muon decay, $\mu^+ \to e^+\gamma\overline{\nu}_\mu\nu_e$, in which both neutrinos are emitted with approximately zero energy; in this case the final state is indistinguishable from that of the signal. It is reduced by requiring the measured e^+ and γ momenta to be opposite in direction and sufficiently close to $m_\mu/2$ that the radiative decay background satisfying these requirements is below the desired sensitivity. A second source of background arises from the accidental overlap of two decays, one providing the γ and the second providing the e^+. The time and spatial coincidence of the particles' origin provide additional background rejection tools. At the stopping intensities required to measure branching fractions below 10^{-12}, the accidental background dominates.

The state of the art is the MEGA experiment [9] at LAMPF. That experiment completed data taking in 1995, and has just reported final results. The total exposure consisted of approximately 1.5×10^{14} stopped muons, and about 5×10^8 events written to tape. Briefly, the detector consists of a set of proportional wire chambers, drift chambers, and scintillation counters in a solenoid. The helical trajectory of electrons are measured in drift and proportional wire chambers. Photons are converted in thin radiators and the trajectories of the resulting e^+e^- pairs measured to deduce the photon momentum. The MEGA result is an upper limit, $\mathrm{B}(\mu^+ \to e^+\gamma) < 1.2 \times 10^{-11}$ at 90% confidence level. This experiment was limited by backgrounds and the reported result is based on a likelihood analysis including signal and background contributions.

The possibility of doing a significantly improved experiment has been dis-

cussed, and a collaboration has submitted a letter of intent [18] to PSI. It is expected that a full proposal will be submitted in late 1999 or early 2000. Currently, different options are being studied for both the electron and photon detector system. It is expected that the sensitivity will be approximately 10^{-14}.

3.2 $\mu^- N \rightarrow e^- N$ Experiments

The principles of an experiment to search for $\mu^- N \rightarrow e^- N$ are quite simple. A beam of μ^- is brought to rest in a thin target. The muons quickly become Coulomb bound to nuclei, and either decay or are captured on the nucleus. For moderate size nuclei, these processes happen at about the same rate, and μ^-'s disappear with a lifetime of about 1 ns. If they convert to electrons, the signature is an isolated electron originating in the stopping target. The basic physics of this process has been studied extensively [19–24]. The process can occur both coherently, with the nucleus left in its ground state, and incoherently, with the nucleus excited [25,26]. The coherent component is large and its magnitude has recently been re-evaluated for various nuclei [16]. The coherence results in an extra factor in the calculation of the rate, equal to Z times the elastic form factor at 105 MeV/c momentum transfer. This enhancement makes $\mu^- N \rightarrow e^- N$ a particularly sensitive probe of LFV processes.

The principal experimental difficulties are getting sufficient μ^- flux and reducing backgrounds due to other sources of 105 MeV electrons. One class of backgrounds is intrinsic, in the sense that they result from μ^- stopped in matter; they can be reduced only by improved electron energy resolution. A second class results from electron, pion and possibly anti-proton contamination in the muon beam and from cosmic rays. These can be reduced or eliminated with a variety of techniques in the beam and detector design. In the case of $\mu^- N \rightarrow e^- N$ experiments, the final state consists of a single particle. Hence, there is no inherent accidental background and the stopping rate can be very high. There may, of course, be backgrounds that are sensitive to rate, those due to energy mismeasurement from pile-up, for example.

The state of the art is the SINDRUM2 experiment [10] at PSI. The first phase is complete, and a limit $R_{\mu e} < 6.1 \times 10^{-13}$ at 90% confidence level has been set. Figure 4 shows a cut view of the apparatus. It is a cylindrical detector, with drift chambers in a solenoid field to measure the e^- momentum. The beam is continuous, and contains a mixture of μ^-'s, π^-'s and e^-'s. About 10^7 μ^-/s are stopped in a target on the axis of the solenoid. Backgrounds from beam contamination are eliminated by rejecting events in which there is a signal in a thin scintillator in the beam that is time coincident with the detected electron. Figure 4 shows the effect of two sets of cuts on the energy

spectrum of electrons. After all cuts are applied, beam and cosmic ray induced backgrounds are eliminated, and the intrinsic background due to μ decay in the Coulomb bound orbit is well separated from the signal region.

The collaboration is working to improve the sensitivity to 4×10^{-14} with a new beam and new background rejection technique. The new μ^- beam [27] is designed to eliminate all π^- and and high momentum e^- from the beam. This will allow the experiment to operate without the beam veto and with the stopping rate increased to $10^8\ s^{-1}$. The basic idea is to reduce the momentum so that muon decay in flight does not result in 105 MeV electrons. Further, the beam is scattered in a thin foil on the axis of a long super-conducting solenoid. Pions that do not decay in the solenoid return to the axis where they are absorbed on a heavy absorber. The proposed beam must reduce π^- and e^- contamination in the beam by a factor of 4000, as deduced from the level of prompt background shown in Fig. 4 and the proposed increase in sensitivity. Currently, the beam is operating, and data is expected to be collected over the next 1-2 years.

The next generation experiment should be designed for a sensitivity below 10^{-16}. The goal would be to explore fully the range of predictions of the grand unified supersymmetric models and provide a very significant reach in parameter space for many non Standard Model scenarios that allow LFV interactions. Reaching this goal will require a much more intense μ^- beam and an experiment with significantly improved background rejection.

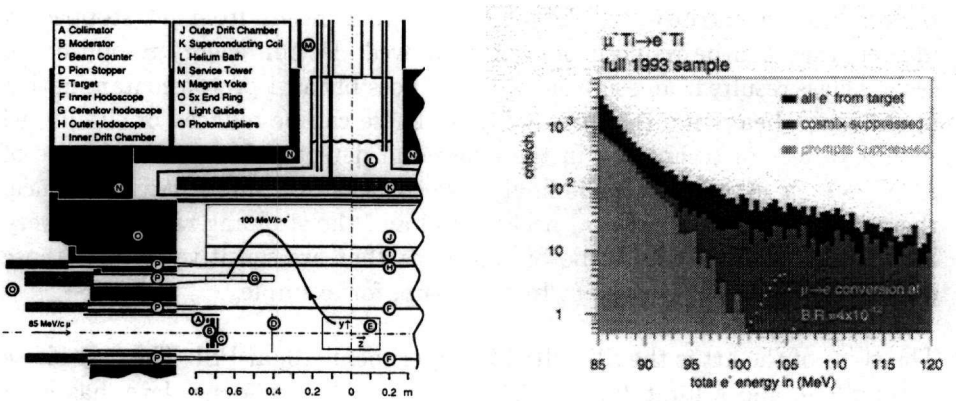

Fig. 4. A cut view of the SINDRUM2 $\mu^- N \rightarrow e^- N$ apparatus is shown on the left. The histogram shows detected electron energy distributions; the lightly shaded contribution is after all cuts have been applied and consists primarily of electrons from muon decay in orbit. The medium shaded region contains background removed by cosmic ray cuts and the heavily shaded area contains prompt background in which the events are removed because a time coincident signal is detected in the beam counter

4 The MECO $\mu^- N \rightarrow e^- N$ Experiment

The Muon to Electron Conversion collaboration has proposed [17] and received scientific approval to do an experiment that will extend the experimental sensitivity for $\mu^- N \rightarrow e^- N$ to below 10^{-16}. It uses a new beam and detector operating at the Brookhaven National Laboratory (BNL) Alternating Gradient Synchrotron (AGS).

The first essential feature of MECO is a very intense μ^- beam. The proposed design uses the idea of Djilkibaev and Lobashev [28,29] to place the π production target in a graded solenoidal field and collect π's over essentially 4π solid angle. They calculated it should be possible to produce up to $\sim 10^{-4}$ μ^- per proton with this design implemented at a high flux, 600 MeV proton accelerator, the Moscow Meson Factory (MMF). Due to circumstances beyond the control of the proponents, this machine will not be able to operate enough to execute a sensitive experiment.

Although AGS has significantly lower current than that proposed for the MMF, its higher energy is particularly advantageous in producing μ^- beams. The AGS currently accelerates 7×10^{13} protons per pulse to 24 GeV. The beam is extracted with 50% duty cycle and has a repetition rate of 3-4 s. The revolution time in the machine is 2.7 ms and it typically operates with 6 RF buckets in the machine. AGS accelerator physicists [30] have devised a method of machine operation using only two bunches, with up to 2×10^{13} protons per bunch (4×10^{13} protons per pulse) with 50% duty factor and 1 second repetition rate. Approximately 0.01 μ^- per proton can be produced at the AGS, resulting in an average flux of a few times 10^{11} μ^-/s . With even more aggressive muon beam design, more than 0.1 μ^- per proton is proposed to be produced at the front end of the muon collider [31,32].

A second essential feature of MECO is the use of a pulsed beam to reduce significantly the prompt backgrounds from π^- and e^- contamination in the beam. Such beams have been used previously in conversion experiments [33]. The basic idea is to produce a pulsed μ^- beam, stop the muons, and then detect conversion electrons only after all π^- and e^- in the beam have either decayed or passed through the detector region. The spacing between pulses must be sufficient to allow all beam particles to disappear and must be comparable to the μ^- lifetime in the stopping target. These considerations lead to a beam pulse frequency of $\sim$1 MHz and the use of an aluminum stopping target, in which the μ^- lifetime is 880 ns. The extinction (ratio of the number of protons between pulses to that in the pulses) is required to be below 10^{-9} to reduce background to negligible levels.

A third critical requirement is a detector system capable of measuring e^-

momenta with high precision in order to minimize intrinsic backgrounds. It must be able to operate in the high rate environment resulting from the high μ^- stopping rate.

A schematic drawing of the MECO beam-line and experimental area is shown in Fig. 5. Pions are produced from a tungsten target in a solenoid; the axial

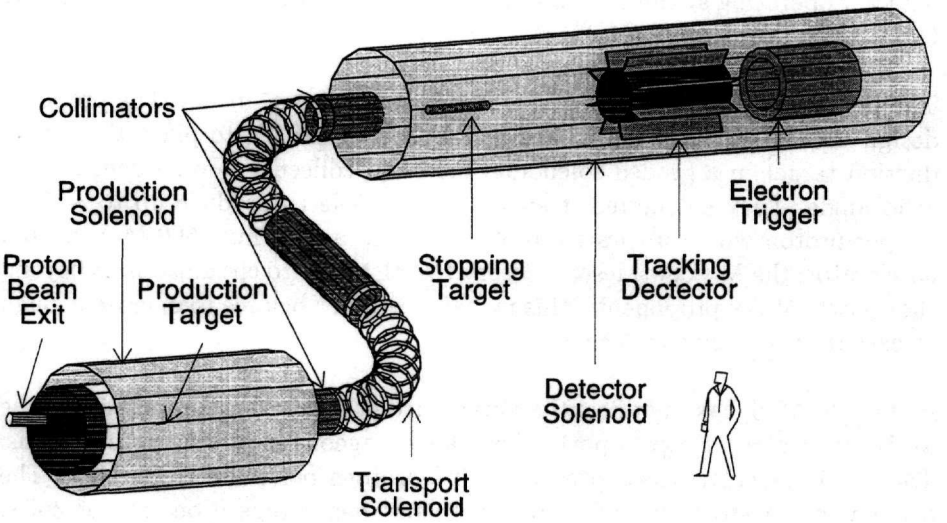

Fig. 5. Schematic drawing of the production solenoid, transport solenoid, and detector solenoid with the targets, collimators, and detectors

component of the field is graded, decreasing from about 4 T at the proton beam exit end to about 2 T at the entrance to the transport solenoid. The graded field results in a very high capture probability for π's and μ's, since charged particles emitted away from the μ^- beam direction are reflected, as in a magnetic bottle. The μ^- beam resulting from π^- decays is transported to the stopping target and detector region in a curved transport solenoid. The effect of the curvature on particles propagating in helical trajectories in the solenoid is exploited to sign and momentum select the beam. This is important for rate and background issues, as will be discussed. The region of the production target, transport, and detector are in vacuum.

The μ^- stopping target and detector are located in a detector solenoid, in which the axial component of the field decreases from 2 T at the entrance to 1 T just after the target. The target consists of 17 disks of aluminum, each with thickness 200 mm and radius ~6 cm. The detector is located downstream of the target in order to minimize rates in it due to particles coming from the target. The use of an axially graded field results in very good acceptance for 105 MeV electrons originating in the target, and allows electrons produced in the upstream pole piece of the production solenoid to be unambiguously distinguished from those produced in the target.

The heart of the detector is the magnetic spectrometer in which the e^- momentum is measured. The tracking detector is low mass in order to minimize the contributions of multiple scattering and energy loss to the electron energy resolution. The electron trigger detector is used to select events to be recorded for off-line analysis by requiring a deposited energy consistent with that of a 105 MeV electron. In addition, it provides some confirmation of the e^- energy, aids in distinguishing e^- from other particles, and helps in identifying backgrounds from particles produced by cosmic rays. The detector region is surrounded by both active and passive cosmic ray shielding (not shown in Fig. 5). This minimizes the rate of production of electrons by cosmic ray muons and allows the identification of e^- that are produced by cosmic rays traversing the detector.

4.1 Physics Background Sources

Physics backgrounds potentially originate from a variety of sources: μ^- decay in a Coulomb bound orbit, radiative μ^- capture, beam electrons, μ^- decay in flight, π^- decay in flight, radiative π^- capture, $\overline{p}$ induced electrons, and cosmic ray induced electrons. The first two are intrinsic to μ^- stopped in the target; they are minimized by measuring the electron energy with high precision. With two exceptions, the other sources derive from prompt processes, with the electron detected close in time to the arrival of a particle in the detector, and are reduced with a pulsed beam. One exception is low energy anti-protons, which have a very long transit time in the muon beam-line and arrive at the stopping target essentially continuously. Hence, they are not significantly reduced by using a pulsed beam. The second exception is cosmic ray background, which is reduced with appropriate active and passive shielding.

The potential sources of backgrounds were studied extensively by the MECO collaboration. Particle production, decay, and interaction in the beam and detector were simulated using the GEANT code package. The simulation included effects of scattering in the beam-line and collimators, inhomogeneities in the magnetic field in the transport region, and energy loss throughout the beam-line. Some processes that are not well modeled by GEANT were calculated with a combination of analytic and Monte Carlo techniques. For example, large angle scattering of electrons in the stopping target was simulated using the Mott scattering formula with nuclear form factors. Rates for some processes (radiative $\pi^-$and μ^- capture, for example) were taken from the literature and incorporated in a Monte Carlo calculation of the background. In the following, the number of background events reported corresponds to an experimental sensitivity of 5 signal events for $R_{\mu e} = 10^{-16}$.

The intrinsic background from μ^- decay in orbit is approximately proportional

to $(E_{max} - E_e)^5$ near the endpoint [34,35]. Hence it is extremely sensitive to both the central part of the detector response function and possible high energy tails. Figure 6 shows the signal and background for $R_{\mu e} = 10^{-16}$, calculated in a full GEANT simulation [36]. By accepting events between 103.9

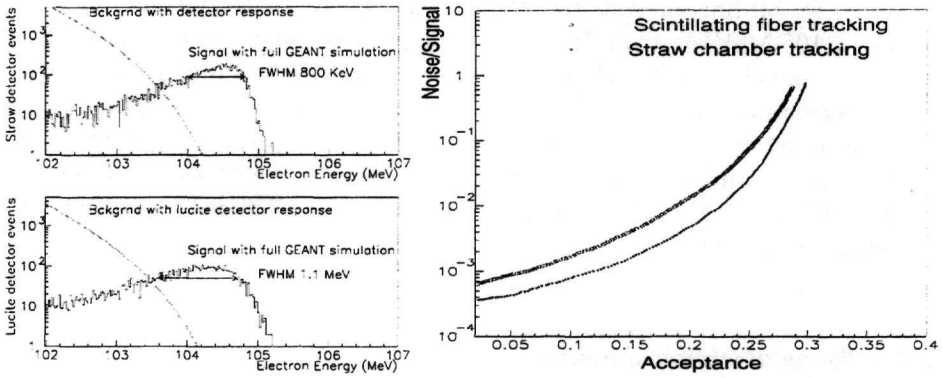

Fig. 6. The histograms on the left show simulations of the expected signal and background for $R_{\mu e} = 10^{-16}$ for two detectors (the upper one corresponds to the detector described in this paper). The normalization of the curves is for $R_{\mu e} = 10^{-16}$ and a luminosity corresponding to 10^7 seconds running time. On the right is a parametric plot of the background/signal and acceptance as a function of the minimum allowed measured e^- energy

MeV and 105.4 MeV, the noise to signal ratio is below 0.05 and the signal acceptance is large.

An additional source of background from muon decay in orbit might result from *pattern recognition errors* when noise signals in the tracking detector are combined with signals from a low energy electron from muon decay in orbit to give a trajectory consistent with a 105 MeV electron. This background source has been independently calculated by superimposing appropriate numbers of noise signals on low energy electron events and searching for all helical trajectories that satisfy appropriate selection criteria, including tracking quality, spatial match of the track projection with the signal in the electron calorimeter, the requirement that all signals on the fitted trajectory be seen, and a requirement that no low momentum track be found. This study is ongoing, and preliminary indications are that the background from this source is negligible if detector rates are at the expected level.

Radiative μ^- capture background results from the $\mu^-\mathrm{Al} \to \gamma\nu_\mu\mathrm{Mg}$ process. The photon endpoint energy is 102.5 MeV and the probability (per μ^- capture) of producing a photon with energy exceeding 100.5 MeV is $\sim 4 \times 10^{-9}$ [37]. The γ conversion probability in the target is $\sim$0.005, and the probability that the electron energy exceeds 100 MeV is $\sim$0.005. The probability of misreconstructing the energy by more than 1.9 MeV is less than 10^{-5}. The background from radiative μ capture is less than 0.05 events.

Beam electrons that cause background are produced in the production or transport solenoid region and then scatter in the stopping target, simulating signal events. The rate for electrons scattering at ~100 MeV/c is defined by the Mott cross section modified by a nuclear form factor. The collimator system is designed to suppress high energy electrons. A GEANT simulation of the production of electrons and their transport to the detector solenoid yielded no transmitted electrons above 100 MeV for 10^7 incident protons. The beam electron background inferred from this calculation is below 0.002 events.

Muon decay in flight can result in energetic electrons that can fake signal. The background from decays in the detector solenoid is below .007 events. Background from π^- decay was also shown by GEANT simulation to be negligible.

Pions stopping in the target are immediately captured by a nucleus and about 2% of them result in the emission of a photon [38] without significant nuclear excitation. The γ energy spectrum has a peak at 110 MeV and endpoint at 140 MeV. The probability of γ conversion in the Al target with a conversion electron in a 1.5 MeV energy interval around 104 MeV is 3.5×10^{-5}. The yield of π's that pass the transport solenoid and stop in the target is $\sim 6 \times 10^{-7}$ per proton. With a beam extinction below 10^{-9}, the background is less than 0.07 events.

A distinct background source is particles that are produced in the main pulse but take a very long time to traverse the production and transport solenoid. The level of this background is difficult to calculate. The suppression factor of 10^{-9} from the beam extinction is absent and this background is suppressed primarily by the small probability that a π^- survives the long transport time. For cases where the π^- does not decay before reaching the stopping target, it was shown by GEANT simulation that this background is below 0.002 events if the detection time starts 0.7 ms after the beam pulse. There are however, special cases, for example in which the π^- decays within the transport solenoid and the muon then scatters at large angle, for which the rate cannot be calculated to sufficient precision due to limited computing resources. In these cases the expected background was calculated using a combination of analytic and Monte Carlo methods. It was found that it is necessary to not have any straight sections in the production or transport solenoids in which the axial component of the field is constant. A design satisfying that requirement has negligible background from particles with long transport times.

Possible background from $\overline{p}$ has been calculated [39] based on measured $\overline{p}$ production cross sections [40,41] at energies near threshold. A nuclear model [42] was used to account for the effects of Fermi motion on the production cross section. The dependence of the production cross section on the $\overline{p}$ momentum was taken from the model, and normalized to the measured cross sections in the forward direction at high momentum. The resulting flux of $\overline{p}$s that con-

tributed to backgrounds was found to be insensitive to the details of the model. It was found that background due to $\overline{p}$ annihilations in the stopping target was significant, and can be suppressed to negligible levels by absorbing the $\overline{p}$s in a thin beryllium window midway through the transport solenoid. The resulting background from π^0 and $\pi^{\pm}$ produced by $\overline{p}$ in the window is below 0.01 events. The background level is sensitive to the proton beam energy and could be reduced further by running at slightly lower energy.

A final potential source of background is cosmic ray induced electrons. This source is unique in that the number of background events is proportional to the data collection time, and not to the sensitivity. Further, improved energy resolution reduces the background, since electrons from cosmic rays will be distributed uniformly in energy in the region of interest. Hence, significant improvement (with respect to that of earlier experiments) in CR induced background rejection is not required. Placing the detector in a graded solenoidal field also provides benefits in reducing background. Most importantly, there is a restricted range of p_T for electrons produced in the stopping target and detected in the spectrometer. This background can be reduced to a level of $\sim$0.004 events per 10^7 seconds of running time with a combination of active and passive shielding and by eliminating events in which extra particles are detected in the tracking detector [43].

4.2 Pulsed Proton Beam

An appropriately pulsed beam is critical to background rejection in MECO. Unlike earlier pulsed beams, the AGS will use the RF structure of the synchrotron to produce the time structure. The operating parameters of the AGS complex are somewhat different than previously used. An acceleration cycle consists of filling two (of six) RF buckets in the AGS lattice in two transfers from the low energy booster, accelerating to 8 GeV, and then resonantly extracting the beam over a 0.5 s spill. Since the beam is held at low energy only for the booster cycle time, higher bunch densities than those currently achieved will be possible. Further, the beam will not be accelerated through transition, also allowing higher bunch density. The beam will then be resonantly extracted over a 0.5 s spill time. This will give a series of narrow ($\ll$ 100 ns) pulses separated by 1.35 ms. It is expected that the intensity will be 4×10^{13} protons per cycle, with a cycle time of 1.0 s and a duty factor of 50%.

Some tests have been made with a bunched beam [44]. One RF bunch was filled, accelerated to 24 GeV, and extracted. Figure 7 shows the relative intensity as a function of time with respect to the filled bunch. The pulses are $\sim$15 ns wide and the extinction between bunches is below 10^{-6} and in unfilled

bunches is of order 10^{-4}. These measurements were made with only minimal tuning of the AGS, and substantially improved performance is expected.

Two ways of improving the extinction have been studied. One involves a set of kickers in the AGS ring that continuously removes beam not in the filled RF buckets [45]. The second involves an external kicker in the extracted proton beam line [46,30]. The internal kicker is the preferred solution, since it operates continuously during the acceleration and extraction and can hence be much lower power.

4.3 Muon Beam Design and Performance

The design of the μ^- production scheme is based on that of the MELC experiment [28,29] and adopted for the muon collider [31,32] source. Pions are produced in a tungsten target in a high field solenoid; those with sufficiently small transverse momentum travel in helical trajectories inside the solenoid and decay to μ's. The field is graded; the axial component varies from 3.3 T at the upstream end to 2 T at the muon beam channel entrance. Muons are transported to the stopping target with good efficiency in a curved solenoid [47] that also removes unwanted particles. It consists of a set of short solenoids arranged to form two bends, each of 90°, surrounded and separated by three straight sections, each containing a collimator. The arrangement is shown in Fig. 5.

Figure 8 shows a schematic drawing of the production solenoid and beginning

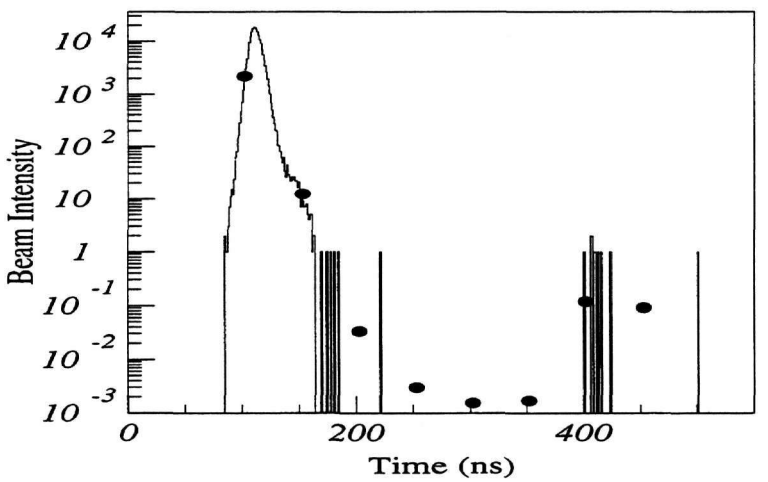

Fig. 7. Plot of the beam intensity as a function of time with respect to pulses in the bunched beam extracted from the AGS. These data were collected without any tuning of the AGS; significantly improved extinction is expected after tuning

of the transport solenoid, on which a typical event is superimposed. The target is a radiation cooled, 0.8 cm diameter, 16 cm long tungsten cylinder. The super-conducting coil is protected with a heat and radiation shield made of tungsten and copper with an inner radius of 0.3 m. The proton beam enters through a hole in the downstream end of the solenoid, and non-interacting protons exit through a larger hole in the upstream end. The direction of the proton beam is opposite that of the muon beam in order to simplify construction of the exit channel and the heat shield, and to minimize the fluence of γ's, neutrons, and $\overline{p}$'s entering the transport solenoid. Low energy pions are produced at all angles, and the use of a graded field minimizes the loss of pions resulting from targeting the protons in the backward direction.

With an incident flux of 2×10^{13} protons per second, the maximum target temperature is below 2450 K [48]. At this temperature the target would lose 0.1% of its mass in a one year run due to evaporation. Incident fluxes a factor of two higher would result in significantly increased evaporation rates, and means of reducing the heat load with different target shapes are being explored. Heat load from the particle spray on the super-conducting solenoid surrounding the production target is manageable based on results of a GEANT calculation [49]. Less than 50 W is deposited in a 6 cm thick coil pack outside the shield. The maximum instantaneous local heat load is below 0.2 mW/gm and the total

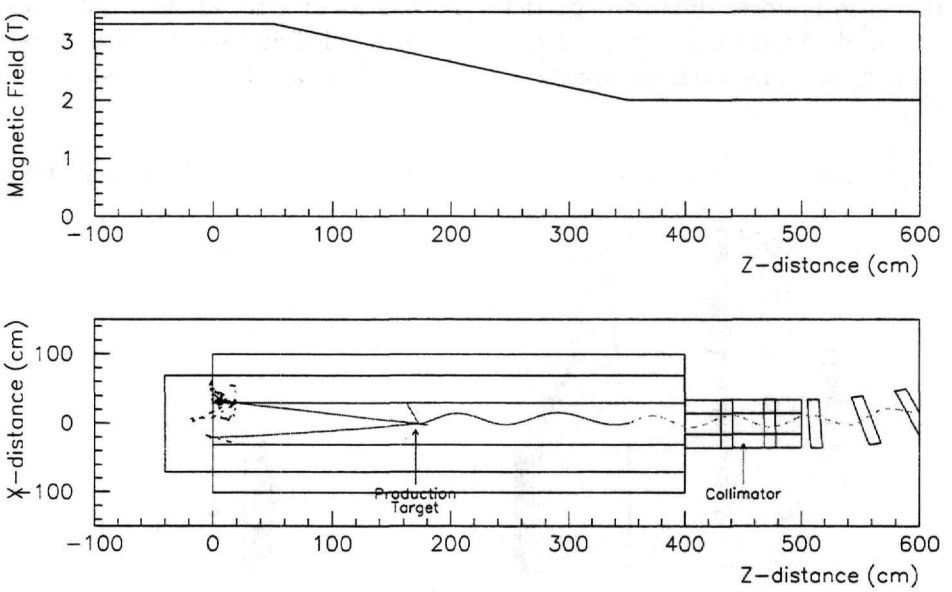

Fig. 8. Schematic drawing of the production solenoid, on which is superimposed a simulated event with a proton interaction producing a μ^-. The incident proton beam enters from the right. Above the drawing is a plot of the axial component of the magnetic field in this region as a function of z. This field has subsequently been modified to remove the regions of constant magnetic field in the production solenoid and first collimator

radiation load in a 10^7 s run is below 50 MRad.

The yield of pions (and hence muons) is calculated [50] based on measurements of the cross section for pion production by 10 GeV protons on tantalum [51]. These data are from an exposure of a bubble chamber with thin tantalum plates within the chamber, and cover the full energy and angular range. The calculation of muon yields for MECO were done by using the GEANT code with the GHEISHA [52] hadron interaction package, and scaling the results by the ratio of measured pion production cross sections to those used used by GHEISHA.

Charged particles are transported to the detector solenoid using a curved solenoid, one purpose of which is to decrease the transmission of positive particles and high momentum negative particles. Charged particles of sufficiently low momentum follow helical trajectories centered on magnetic field lines. In a torus, they drift in a direction perpendicular to the plane of the torus, by an amount given by $D = 1/0.3 \times B \times s/R \times (p_s^2 + \frac{1}{2}p_t^2)/p_s$, where D is the drift distance, B is the magnetic field, s/R is the bend angle of the solenoid, and p_t and p_s are the perpendicular and parallel momentum components. For $s/R = \pi/2, p_t = 0.09$ GeV/c, $p_s = 0.12$ GeV/c, and $B = 2$ T, the drift of the center of the helix is 49 cm. The drift direction depends on the charge; this is illustrated in Fig. 9. Collimators that remove most positive particles and all negative particles above 100 MeV/c are placed in the straight sections (shown in Fig. 9). The results of the calculations of muon yields are discussed in the section on expected MECO sensitivity.

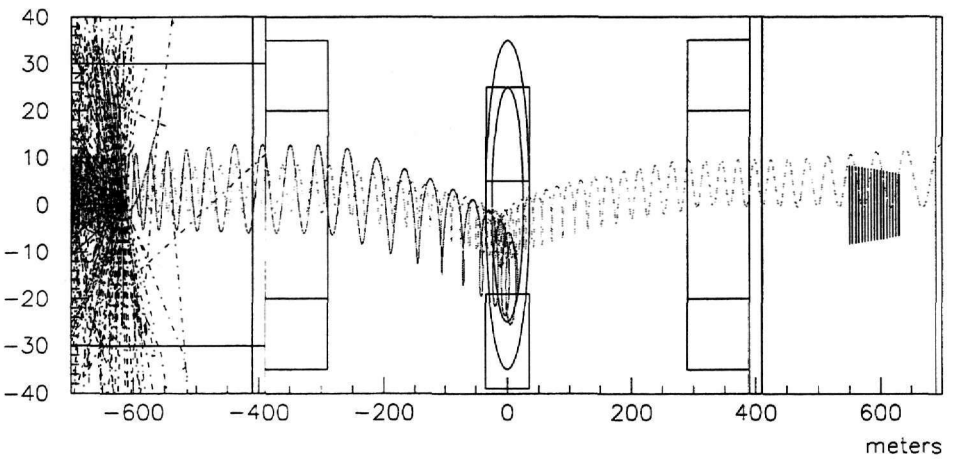

Fig. 9. A side view of the production, transport and detector solenoids, with a simulation of a number of proton interactions superimposed. The effect of the curvature drift is seen in the regions in the horizontal coordinate between -300 and +300. Negative particles first drift down in the first curved section, are collimated in the central collimator, and then drift back up in the second curved section

The stopping target and detectors are located in a solenoid of radius ~.9 m, with a graded axial field, decreasing from 2T at the entrance to 1 T between the stopping target and detectors, after which it remains constant. The use of a graded field has two consequences. First, the quantity p_T^2/B_Z is constant, and hence 105 MeV e^-, either in the beam or produced at the upstream end of the solenoid, will have $p_T < 74$ MeV/c at the detector and can be eliminated as background by requiring $p_T > 75$ MeV/c. Second, conversion electrons emitted at angles of $90° \pm 30°$ with respect to the solenoid axis will have trajectories that intercept the tracking detector and that have a restricted range of p_T. Those initially moving away from the detector bounce in the graded field. This allows the tracking detector to be in a uniform field region displaced from the stopping target, which minimizes rates in that detector. Sample trajectories illustrating this are shown in Fig. 10.

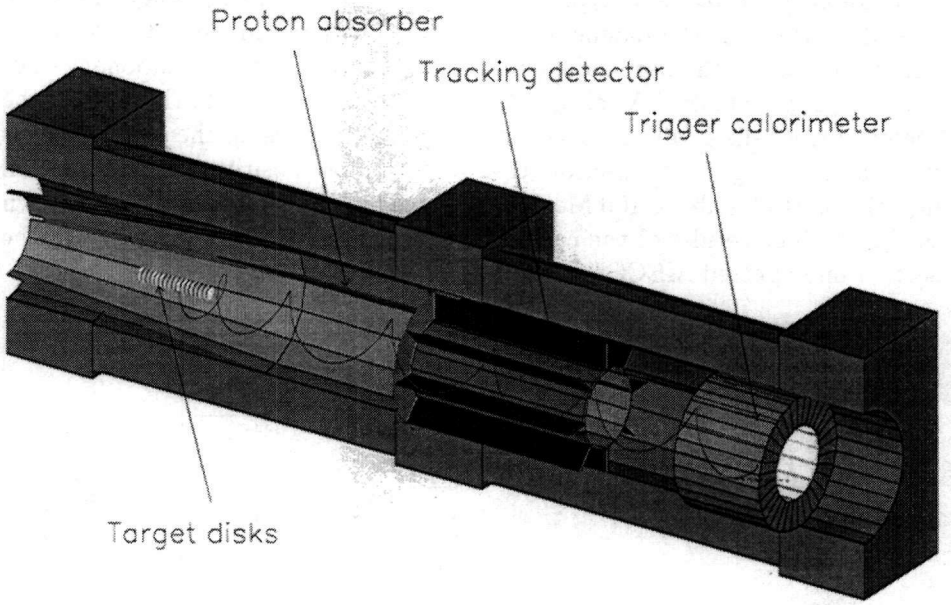

Fig. 10. A schematic representation of the MECO detector region from the GEANT simulation, with a typical conversion electron trajectory produced by the GEANT simulation superimposed

The goal for the tracking detector is to measure with good efficiency the parameters of the helical trajectory of electrons. The detector consists of a cylinder and 8 equally spaced *vanes* of tracking detectors, as shown in Fig. 5. All individual detector elements are oriented in the axial direction. The baseline design of the cylinder and vanes uses three layers of 5 mm diameter, 2 m long straw tubes. The straws will be made from carbon-loaded kapton to

provide an electrically semi-transparent structure. The axial coordinate will be measured using copper pads etched on kapton foil and placed in contact with the straws.

The uncertainty in the momentum measurement is dominated by multiple scattering and the design has been optimized to minimize the material. The performance of the detectors was calculated using a full GEANT simulation of the stopping target and detectors [36]. It incorporated the Moliere scattering formalism and Landau fluctuations in the energy loss. It used Gaussian measurement errors with σ_x, σ_y and σ_z equal to 0.2 mm, 0.2 mm and 1.4 mm, respectively. This spatial resolution is easily achieved in straw chamber technology. Figure 10 shows a few typical events in the simulation.

To ensure that the events have well measured trajectories, only events with at least three clusters of hits in a single helical turn and five total clusters are used. A trajectory that goes through all clusters of hits is calculated using a maximum likelihood method. It determines the trajectory connecting each pair of hit segments as a function of the electron momentum, p_e, and then maximizes the likelihood, $L(p_e)$, as a function of p_e; $L(p_e)$ is the product of the scattering probabilities at each detector position. The uncertainty in the fit is derived from the shape of the likelihood function in the region of the peak. The σ_{RMS} is 170 keV; including the effect of energy loss straggling in the stopping target and proton absorbers increases this to a FWHM of 750 keV with a low energy tail. To select signal events, suitable requirements on the fitting quality were applied and the electron energy and p_T were required to exceed 103.9 MeV and 75 MeV/c. From these simulations, the acceptance of the detector and analysis scheme was determined; this is discussed in the section on the expected sensitivity of MECO.

Using the resolution function determined from Monte Carlo simulated events, the level of muon decay in orbit background was calculated [36] by convolving the resolution function with the theoretical background electron energy spectrum. Figure 6 shows the noise to signal ratio vs. acceptance for the two detector possibilities, parameterized as a function of the lower edge of the accepted electron energy range. This and other background contributions are summarized in the section on the expected sensitivity of MECO.

The purpose of the electron trigger calorimeter in the MECO experiment is to detect electrons with ~105 MeV energy that have passed through the tracking system and to provide a second, lower resolution measurement of the electron energy. Two detector technologies are being considered [53,54]. One uses a a pure plastic scintillator cylinder of outer radius 70 cm, inner radius 41 cm, and 1 m length, segmented in azimuthal angle and axially. A second possible implementation uses a number of *vanes* of crystal scintillator.

The rate of events satisfying a minimum energy requirement in the electron calorimeter will be dominated by the high energy tail of e^- from muon decay in orbit. This rate has been estimated by convolving the electron energy distribution with the response function of the calorimeter and imposing a minimum energy requirement of 65 MeV. Without the effects of pile-up of photons and neutrons, the trigger rate is ~1.0 kHz. The rate with pile-up is expected to be below 10kHz.

Finally, the region of the detector solenoid is shielded from cosmic rays with a combination of active and passive shielding. It consists of 0.5 m of steel (some of which is provided by the return yoke of the magnet) surrounding the detector solenoid, two layers of plastic scintillator, and 2 m of concrete shielding. The scintillator veto shield contains ~300 m^2 of scintillator; one possible implementation is to use extruded plastic scintillator similar to that now intended to be used in the MINOS neutrino detector.

The cosmic ray induced background was calculated [43] using measured cosmic ray fluxes [55,56] and a GEANT simulation of the shielding and detector. Muons dominate the flux of particles penetrating any significant amount of shielding. The rate of background induced by cosmic rays in which no charged particle traverses the active veto is very small; additionally, it is assumed that the probability of not detecting a through-going charged particle in either layer of scintillator is 10^{-4}. The calculation accounts for electrons produced by muons penetrating the shielding and decaying in the detector solenoid or interacting in the target and detectors. Particles were eliminated as potential background based on selection criteria including the measured momentum, p_T, charge, projection to the muon stopping target, fitting quality, number of detector elements with signals expected but missing, and energy deposited in the electron trigger detector.

In a simulation equivalent to ~200 years exposure, three events satisfied all selection criteria, corresponding to a cosmic ray induced background of 0.0035 events in 10^7 seconds of exposure.

4.5 Expected Performance and Sensitivity of MECO

The sensitivity that will be achieved by MECO depends on the running time, proton intensity, number of muons per proton produced and transported to the stopping target, stopping probability, fraction of stops that capture rather than decay, trigger efficiency, accidental cosmic ray veto loss, tracking acceptance, and losses due to analysis inefficiencies and background rejection selection criteria. The values of the acceptance and efficiency for these are given in Table 2. Loss of events due to accidental cosmic ray vetos and dead-time

losses are expected to be small; losses in pattern recognition in the tracking detector are also expected to be small but have not yet been calculated precisely. In one year (10^7 s) running time, a few events will be detected at a value of $R_{\mu e} = 10^{-16}$.

Table 3 shows the expected background rates for the sensitivity quoted above. The background is dominated by the μ^- decay in orbit contribution. Substantial improvement in discrimination against this source of background can

Table 2
A summary of the expected MECO sensitivity for a one year (10^7 s) run

Running time (sec)	10^7
Proton flux (sec^{-1}) (50% DF, 1.35 ms bunch spacing)	4×10^{13}
μ/p entering solenoid	0.006
Stopping probability	0.370
μ capture probability	0.600
Fraction of μ that capture in time window	0.480
Electron trigger efficiency	0.900
Fitting and selection criteria	0.250
Detected events for $R_{\mu e} = 10^{-16}$	5.800

Table 3
A summary of the level of background from various sources, calculated for the sensitivity given in the previous table, and with scaling as discussed in the text

Source	Events	Comment
μ decay in orbit	0.29	signal/noise = 20 for $R_{\mu e} = 10^{-16}$
Radiative μ capture	$\ll 0.050$	
μ decay in flight	$< 0.030 \times \frac{\varepsilon}{10^{-9}}$	without scatter in target
μ decay in flight	$0.040 \times \frac{\varepsilon}{10^{-9}}$	with scatter in target
Radiative π capture	$0.070 \times \frac{\varepsilon}{10^{-9}}$	from proton during detection time
Radiative π capture	0.014	from late arriving π
π decay in flight	$\ll 0.010 \times \frac{\varepsilon}{10^{-9}}$	
Beam electrons	$< 0.020 \times \frac{\varepsilon}{10^{-9}}$	
$\overline{p}$ induced	0.004	
Cosmic ray induced	0.004	assuming 10^{-4} CR veto inefficiency
Total background	0.420	assuming 10^{-9} extinction

be had with modest loss in acceptance, as shown in Fig. 6. For example, the background/signal ration can be decreased from 0.05 to 0.02 with a relative loss in sensitivity of less than 10%.

Many of the backgrounds depend on the proton beam extinction, and we have given the calculated background level scaled by this extinction. An extinction at or below 10^{-9} is sufficient to reduce these backgrounds to negligible levels. At the proposed sensitivity, the experiment is not expected to be limited by background.

4.6 MECO Cost and Schedule

The current MECO cost estimate is based on a variety of methods, most involving comparison with existing technology. It is dominated by the three super-conducting solenoids in the muon beam line and their refrigerator. These costs are estimated based on those of large thin-coil solenoids [57]. The budget for magnets and refrigerator is \$20M. Other large cost items are the proton beam-line, preparation of the experimental area (\$3.0M), the internal and external kickers to provide the requisite beam extinction (\$2.6M), and the muon production target and the production solenoid radiation shield (\$0.9M). The largest contribution to the cost of the experiment is for electronics (\$3.0M) for the various detectors. The total current cost estimate is \$32.4M. More precise costing requires engineering design, in particular that of the super-conducting solenoids.

The duration of the construction phase of the experiment is determined by the time to design, build and install the unique muon beam line. While none of the individual components of this beam-line are beyond the state of the art of the respective technologies, there are a lot of pieces that require substantial technical design before construction can begin. The critical path item is the set of super-conducting solenoids, preliminary design work of these devices has begun and it is expected that the design and construction would take three years.

It is anticipated that MECO could be built by the end of 2002, given appropriate funding and that data will be collected in 2003 and 2004 for a total of 4000 hours, which could be achieved in 40 weeks of AGS operation.

5 Summary

Experiments to search for violation of muon and electron number have now been done for over 40 years, with ever increasing sensitivity. With the exception of the recent evidence for neutrino oscillations, no indication of LFV processes has been seen. Current limits on muon induced processes are at the level of 10^{-11} for $\mu^+ \to e^+\gamma$ and 10^{-12} for $\mu^+ \to e^+e^+e^-$ and $\mu^-N \to e^-N$. These limits place stringent constraints on many scenarios for physics beyond the Standard Model.

Improvements in muon beams and detector technology hold promise for making further significant improvements in the sensitivity of searches in the next few years. In particular, the SINDRUM2 experiment being done at the PSI laboratory is expected to improve the sensitivity to $\mu^-N \to e^-N$ to below 10^{-13} in the next year or two. Further improvement, to a sensitivity below 10^{-16}, is promised by the MECO experiment, now approved at BNL. Ideas have been discussed for improving the sensitivity to $\mu^+ \to e^+\gamma$ to near 10^{-14} with an experiment at PSI. When these experiments are done, they will be sensitive to the level of lepton flavor violating signals suggested in many scenarios for physics beyond the Standard Model. In particular, predictions of a class of grand unified supersymmetric models will be confronted directly by experimental measurements. The very substantial expected improvement in experimental sensitivity, coupled with the predictions of grand unified supersymmetric models, allow some optimism that the first evidence for muon and electron number violation may be found.

Acknowledgments

I thank the organizers of this meeting in honor of John Vergados for the stimulating program in a very pleasant environment and for their support to allow me to attend. I thank Andries vanderSchaaf for information on the SINDRUM2 experiment, Ed Hungerford and Martin Cooper for information on MEGA, and my collaborators on MECO for their contributions to the experiment.

References

[1] Y. Fukuda *et al.*, Phys. Rev. Lett. **81**, 1562 (1998).

[2] Y. Fukuda *et al.*, Phys. Rev. Lett. **82**, 2644 (1999).

[3] C. Athanassopoulos *et al.*, Phys. Rev. Lett. **81**, 1774 (1998).

[4] R.N. Cahn and H. Harari, Nucl. Phys. **B176**, 135 (1980).

[5] D. Ambrose *et al.*, Phys. Rev. Lett. **81**, 5734 (1998).

[6] P. Krolak *et al.*, Phys. Lett. **B320**, 407 (1994).

[7] A.M. Lee *et al.*, Phys. Rev. Lett. **64**, 165 (1990).

[8] U. Bellgardt *et al.*, Nucl. Phys. **B299**, 1 (1988).

[9] M.L. Brooks *et al.*, *New limit for the family number nonconserving decay* $\mu^+ \to e^+\gamma$, Los Alamos preprint LA-UR-99-2268, submitted to Phys. Rev. Lett., 1999.

[10] F. Riepenhausen, in *Proceedings of the Sixth Conference on the Intersections of Particle and Nuclear Physics*, edited by T. Donnelly (American Institute of Physics, New York, 1997), p. 34.

[11] W. Marciano, Nucl. Phys **B59**, 34 (1997).

[12] J. Hisano *et al.*, Phys. Lett. **B391**, 347 (1997).

[13] R. Barbieri and L.J. Hall, Nucl. Phys. **B338**, 212 (1994).

[14] R. Barbieri, L. Hall, and A. Strumia, Nucl. Phys. **B445**, 219 (1995).

[15] N. Arkani-Hamed, H.C. Cheng, and L.J. Hall, Phys. Rev. **D53**, 413 (1996).

[16] A. Czarnecki, W. Marciano, and K. Melnikov, in *Workshop on Physics at the First Muon Collider and at the Front End of the Muon Collider*, edited by S. H. Geer and R. Raja (American Institute of Physics, Woodbury, N.Y., 1998), p. 409.

[17] M. Bachman *et al.*, *A Search for* $\mu^- N \to e^- N$ *with Sensitivity Below* 10^{-16}, BNL AGS Proposal 940, 1997.

[18] S. Korenchenko *et al.*, *Search for the Decay* $\mu^+ \to e^+\gamma$ *with a Branching Ratio Sensitivity of* 10^{-14}, PSI Letter of Intent, 1998.

[19] S. Weinberg and G. Feinberg, Phys. Rev. Lett. **3**, 111 (1959).

[20] N. Cabibbo and R. Gatto, Phys. Rev. **116**, 1334 (1959).

[21] S.P. Rosen, Nuovo Cim. **15**, 7 (1960).

[22] W. Marciano, Phys. Rev. Lett. **38**, 1512 (1977).

[23] T.S. Kosmas and J.D. Vergados, Phys. Lett. **B217**, 19 (1989).

[24] T.S. Kosmas and J.D. Vergados, Phys. Rep. **264**, 251 (1996).

[25] T.S. Kosmas, A. Faessler, F. Simkovic, and J.D. Vergados, Phys. Rev. **C56**, 526 (1997).

[26] J. Schwieger, T.S. Kosmas, and A. Faessler, Phys. Lett. **B443**, 7 (1998).

[27] M. Rutsche, Ph.D. thesis, University of Zurich, 1996.

[28] R. Djilkibaev and V.M. Lobashev, Sov. J. Nucl. Phys. **49(2)**, 384 (1989).

[29] V.S. Abadjev *et al.*, *MELC Experiment to Search for the* $\mu^- A \rightarrow e^- A$ *Process*, INR preprint 786/92, 1992.

[30] J.S.A. Soukas and W. Meng, Technical report, Brookhaven National Laboratory (unpublished).

[31] J.C. Gallardo (ed.), in *Beam dynamics and technology issues for mu+ mu- colliders*, Proceedings, 9th Advanced ICFA Beam Dynamics Workshop, Montauk, USA, October 15-20, 1995 (American Institute of Physics, Woodbury, N.Y., 1996), p. 372.

[32] R. Palmer *et al.*, Nucl. Phys. Proc. Suppl. **51A**, 61 (1996).

[33] A. Badertscher *et al.*, Nucl. Phys. **A377**, 406 (1979).

[34] O. Shanker, Phys. Rev. **D20**, 1608 (1979).

[35] O. Shanker, Phys. Rev. **D25**, 1847 (1982).

[36] T.J. Liu, meco- 004, University of California, Irvine (unpublished).

[37] A. Frischknecht *et al.*, Phys. Rev. **C2**, 1506 (1985).

[38] R.A. Eramzhyan *et al.*, Nucl. Phys. **A290**, 294 (1977).

[39] T.J. Liu, meco- 026, University of California, Irvine (unpublished).

[40] B. Cork *et al.*, Phys. Rev. **107**, 248 (1957).

[41] G.J. Marmer *et al.*, Phys. Rev. **179**, 1294 (1969).

[42] O. Benhar, A. Fabrocini, S. Fantoni, and I. Sick, Nucl. Phys. **A579**, 493 (1994).

[43] M. Overlin, meco- 014, University of California, Irvine (unpublished).

[44] R. Lee, meco- 017, University of California, Irvine (unpublished).

[45] A. Soukas, 1998, private communication.

[46] W. Molzon, meco 006, University of California, Irvine (unpublished).

[47] W. Molzon, meco- 008, University of California, Irvine (unpublished).

[48] R. Djilkibaev, meco- 010, University of California, Irvine (unpublished).

[49] W. Molzon, meco- 018, University of California, Irvine (unpublished).

[50] R. Djilkibaev, meco- 023, University of California, Irvine (unpublished).

[51] D. Artmutliski *et al.*, Sov. J. Nucl. Phys. **48**, 161 (1988).

[52] H. C. Fesefeldt, Technical report, University of Achen, (unpublished), report PITHIA 85-02.

[53] S. Carabello and D. Koltick, meco- 015, Purdue University (unpublished).

[54] J. Sculli, meco- 022, New York University (unpublished).

[55] O. Allkofer *et al.*, Phys. Lett. **36B**, 425 (1971).

[56] O.C. Allkofer *et al.*, Nucl. Phys. **B259**, 1 (1985).

[57] R.A.B. M.A. Green and S.J.S. Lorant, Adv. in Cry. Eng. **37**, (1992).